Monthly Notices
of the
ROYAL ASTRONOMICAL SOCIETY

Mon. Not. R. Astron. Soc. **419,** 2844–2854 (2012) doi:10.1111/j.1365-2966.2011.19925.x

# Local stellar kinematics from RAVE data – II. Radial metallicity gradient

B. Coşkunoğlu,[1⋆] S. Ak,[1] S. Bilir,[1] S. Karaali,[1] Ö. Önal,[1] E. Yaz,[1] G. Gilmore[2,3] and G. M. Seabroke[4]

[1]*Istanbul University, Science Faculty, Department of Astronomy and Space Sciences, 34119 University-Istanbul, Turkey*
[2]*Institute of Astronomy, Madingley Road, Cambridge CB3 OHA*
[3]*Astronomy Department, Faculty of Science, King Abdulaziz University, PO Box 80203, Jeddah 21589, Saudi Arabia*
[4]*Mullard Space Science Laboratory, University College London, Hombury St Mary, Dorking RH5 6NT*

Accepted 2011 September 29. Received 2011 September 27; in original form 2011 August 16

## ABSTRACT

We investigate radial metallicity gradients for a sample of dwarf stars from the RAdial Velocity Experiment (RAVE) Data Release 3 (DR3). We select a total of approximately 17 000 F-type and G-type dwarfs, using a selection of colour, $\log g$ and uncertainty in the derived space motion, and calculate for each star a probabilistic (kinematic) population assignment to a thick or thin disc using space motion and additionally another (dynamical) assignment using stellar vertical orbital eccentricity. We additionally subsample by colour, to provide samples biased toward young thin-disc and older thin-disc stars. We derive a metallicity gradient as a function of Galactocentric radial distance, i.e. $\mathrm{d}[M/\mathrm{H}]/\mathrm{d}R_\mathrm{m} = -0.051 \pm 0.005\,\mathrm{dex\,kpc^{-1}}$, for the youngest sample, F-type stars with vertical orbital eccentricities $e_\mathrm{v} \leq 0.04$. Samples biased toward older thin-disc stars show systematically shallower abundance gradients.

**Key words:** stars: abundances – Galaxy: abundances – Galaxy: disc – Galaxy: evolution.

## 1 INTRODUCTION

Abundance gradients in galactic discs are an important constraint on star formation and interstellar medium history and the possible secular evolution of stars post-formation in those discs. In the Milky Way Galaxy, there is extensive information establishing a radial gradient in young stars and in the interstellar medium (Shaver et al. 1983; Luck, Kovtyukh & Andrievsky 2006; Luck & Lambert 2011). Values typically derived are $\mathrm{d[Fe/H]}/\mathrm{d}R_\mathrm{G} = -0.06 \pm 0.01\,\mathrm{dex\,kpc^{-1}}$, within 2–3 kpc of the Sun. A concerted effort to search for local abundance variations and abundance variations with azimuth shows little, if any, detectable variation in young systems (Luck et al. 2011), limiting the importance of radial gas flows.

Quantifying the abundance distribution functions and their radial and vertical gradients in both thin and thick discs can be achieved using stellar abundances, especially those from major surveys such as the RAdial Velocity Experiment (RAVE: Steinmetz et al. 2006; Zwitter et al. 2008; Siebert et al. 2011). Several recent analyses of RAVE data have studied the metallicity and kinematics of Galactic disc distribution functions from RAVE data (Burnett et al. 2011; Ruchti et al. 2011; Wilson et al. 2011; Karataş & Klement 2012).

Even more fundamental is the variation of the abundance gradient with time. Some information is available, especially from open star clusters and field stars. The evidence here suggests that the gradient flattens beyond about 12 kpc Galactocentric radius (Carney et al. 2005; Yong, Carney & Teixera de Almeida 2005), as is seen in other spiral galaxies (Worthey et al. 2005; Vlajić, Bland-Hawthorn & Freeman 2009). At the outermost radii, the situation may be more complex.

The observational situation, however, can be improved. Extant data suggest vertical metallicity gradients in the $-0.4 < \mathrm{d}[M/\mathrm{H}]/\mathrm{d}z < -0.2\,\mathrm{dex\,kpc^{-1}}$ range for relatively small distances from the Galactic plane, i.e. $z < 4$ kpc (Trefzger, Pel & Gabi 1995; Karaali et al. 2003; Du et al. 2004; Ak et al. 2007a). For intermediate $z$ distances, where the thick disc is dominant, the vertical metallicity gradient is low, $\mathrm{d}[M/\mathrm{H}]/\mathrm{d}z = -0.07\,\mathrm{dex\,kpc^{-1}}$, and the radial gradient is only marginal, $-0.02 \leq \mathrm{d}[M/\mathrm{H}]/\mathrm{d}z \leq 0\,\mathrm{dex\,kpc^{-1}}$ (Rong, Buser & Karaali 2001). There is some evidence that metallicity gradients for relatively short vertical distances, $z < 2.5$ kpc, show systematic fluctuations with Galactic longitude, similar to those of the thick-disc scaleheight, which may be interpreted as a common flare effect of the disc (Ak et al. 2007b; Bilir et al. 2008; Yaz & Karaali 2010).

These vertical gradients are perhaps a convolution of a time-dependent abundance and the well-established stellar age–velocity dispersion relation. Alternatively, they may be more consistent with two independent, rather narrow metallicity distributions: one thin disc, one thick disc, with the apparent gradient being simply a reflection of the two different scaleheights (Gilmore & Wyse 1985; Burnett et al. 2011).

In this study we analyse stellar abundance gradients from RAVE data, using colour bins as a proxy for mean age, to test for time-dependent effects. RAVE is a multifibre spectroscopic astronomical

⋆E-mail: basarc@istanbul.edu.tr

© 2011 The Authors
Monthly Notices of the Royal Astronomical Society © 2011 RAS

Downloaded from https://academic.oup.com/mnras/article-abstract/419/4/2844/2908030 by guest on 28 January 2020

survey of stars in the Milky Way, which covers just over half of the Southern hemisphere using the 1.2-m UK Schmidt Telescope of the Australian Astronomical Observatory (AAO). RAVE's primary aim is to derive the radial velocity of stars from the observed spectra for solar neighbourhood stars. Additional information is also derived, such as photometric parallax and stellar atmospheric parameters, i.e. effective temperature, surface gravity, metallicity and elemental abundance data. This information is important in calculating metallicity gradients, which provide data about the formation and evolution of the Galaxy. As the data were obtained from solar-neighbourhood stars, we have limitations on the distance and range of metallicity. However, the metallicity measurements are of high internal accuracy, which is an advantage for our work. A radial metallicity gradient of $-0.04\,\mathrm{dex\,kpc^{-1}}$, based on calibrated metallicities from the RAVE DR2 data, has already appeared in the literature (Karataş & Klement 2012). However, this metallicity gradient covers all spectral types, and thus a wide age range, which is a disadvantage for a sample of stars with distance and metallicity range restrictions. Hence, in this study we will use only the data for F and G spectral-type stars. We test for different metallicity gradients for different spectral types.

The structure of this paper is as follows. Data selection is described in Section 2, while calculated space velocities and orbits of star samples and population analysis are described in Sections 3 and 4, respectively. Results are given in Section 5 and a summary and conclusions are presented in Section 6.

## 2 DATA

The data were selected from the third data release of RAVE (DR3: Siebert et al. 2011). RAVE DR3 reports 83 072 radial velocity measurements for stars with $9 \leq I \leq 12$. This release also provides stellar atmospheric parameters for 41 672 spectra representing 39 833 individual stars (Siebert et al. 2011). The accuracy of the radial velocities is high, marginally improved with DR3: the distribution of internal errors in the radial velocities has a mode of $0.8\,\mathrm{km\,s^{-1}}$ and a median of $1.2\,\mathrm{km\,s^{-1}}$, while 95 per cent of the sample has an internal error smaller than $5\,\mathrm{km\,s^{-1}}$. The uncertainties in the stellar atmospheric parameters are 250 K for effective temperature $T_{\rm eff}$, 0.43 dex for surface gravity $\log g$ and 0.2 dex for [*M*/H]. While RAVE supports a variety of chemical abundance scales, we use here just the public DR3 values. Since anticipated gradients are small, this provides a well-defined set of parameters for analysis.

A surface gravity constraint $4 < \log g \leq 5$ was applied to the 83 072 star sample to obtain a homogeneous dwarf star subsample with accurate data. Distances of the subsample stars were obtained using the absolute magnitude calibration of Bilir et al. (2008), whereas the reddening values were obtained iteratively, following published methodology (for more detailed information regarding the iterations see Coşkunoğlu et al. 2011, and the references therein).

Our aim here is to take advantage of RAVE's focus on high Galactic latitude to isolate statistically the samples dominated by thin-disc and thick-disc stars. Thus, after dereddening, stars were split into F and G spectral-type subsamples using Straizys & Lazauskaite (2009)'s criteria, i.e. $0.09 < (J-H)_0 \leq 0.29$ and $0.29 < (J-H)_0 \leq 0.39$, leaving us with 17 768 stars. Out of these 17 768 stars, 10 661 are F- and 7107 are G-type dwarfs, while the sample median distances are 326 and 272 pc, respectively.

## 3 SPACE VELOCITIES AND ORBITS

We combined the distances estimated in Section 2 with RAVE kinematics and the available proper motions, applying the (standard) algorithms and the transformation matrices of Johnson & Soderblom (1987) to obtain their Galactic space-velocity components (*U*, *V*, *W*). In the calculations, epoch J2000 was adopted as described in the International Celestial Reference System (ICRS) of the *Hipparcos* and *Tycho-2* Catalogues (ESA 1997). The transformation matrices use the notation of a right-handed system. Hence, *U*, *V* and *W* are the components of a velocity vector of a star with respect to the Sun, where *U* is positive towards the Galactic centre ($l = 0^\circ$, $b = 0^\circ$), *V* is positive in the direction of Galactic rotation ($l = 90^\circ$, $b = 0^\circ$) and *W* is positive towards the North Galactic Pole ($b = 90^\circ$).

Correction for differential Galactic rotation is necessary for accurate determination of *U*, *V* and *W* velocity components. The effect is proportional to the projection of the distance to the stars on to the Galactic plane, i.e. the *W* velocity component is not affected by Galactic differential rotation (Mihalas & Binney 1981). We applied the procedure of Mihalas & Binney (1981) to the distribution of the sample stars and estimated the first-order Galactic differential rotation corrections for the *U* and *V* velocity components of the sample stars. The range of these corrections is $-25.71 < \mathrm{d}U < 16.92$ and $-1.57 < \mathrm{d}V < 2.29\,\mathrm{km\,s^{-1}}$ for *U* and *V*, respectively. As expected, *U* is affected more than *V*. Also, the high values for the *U* component show that corrections for differential Galactic rotation cannot be ignored.

The uncertainties in the space-velocity components $U_{\rm err}$, $V_{\rm err}$ and $W_{\rm err}$ were computed by propagating the uncertainties in the proper motions, distances and radial velocities, again using a (standard) algorithm by Johnson & Soderblom (1987). Then, the error for the total space motion of a star follows from the equation

$$S_{\rm err}^2 = U_{\rm err}^2 + V_{\rm err}^2 + W_{\rm err}^2. \quad (1)$$

The median and standard deviation for space velocity errors are $\tilde{\rm S}_{\rm err} = 8.01\,\mathrm{km\,s^{-1}}$ and $s = 16.99\,\mathrm{km\,s^{-1}}$, respectively. We now remove the most discrepant data from the analysis, knowing that outliers in a survey such as this will preferentially include stars that are systematically misanalysed binaries, etc. Astrophysical parameters for such stars are also likely to be relatively unreliable. Thus, we omit stars with errors that deviate by more than the sum of the standard error and the standard deviation, i.e. $S_{\rm err} > 25\,\mathrm{km\,s^{-1}}$. This removes 760 stars, ∼4.3 per cent of the sample. Thus, our sample was reduced to 17 008 stars, those with more robust space-velocity components. After applying this constraint, the median values and the standard deviations for the velocity components were reduced to $(\tilde{U}_{\rm err}, \tilde{V}_{\rm err}, \tilde{W}_{\rm err}) = (3.93 \pm 3.10, 3.59 \pm 2.79, 3.16 \pm 2.75)\,\mathrm{km\,s^{-1}}$.

To complement the chemical abundance data, accurate kinematic data have been obtained and used to calculate individual Galactic orbital parameters for all stars. In order to calculate those parameters, we used standard gravitational potentials that are well described in the literature (Miyamoto & Nagai 1975; Hernquist 1990; Johnston, Spergel & Hernquist 1995; Dinescu, Girard & van Altena 1999) to estimate the orbital elements of each of the sample stars. The orbital elements for a star used in our work are the mean of the corresponding orbital elements calculated over 15 orbital periods of that specific star. The orbital integration typically corresponds to 3 Gyr, and is sufficient to evaluate the orbital elements of solar-neighbourhood stars, most of which have orbital periods below 250 Myr.

Solar-neighbourhood velocity space includes well-established substructures that resemble classic moving groups or stellar streams

Downloaded from https://academic.oup.com/mnras/article-abstract/419/4/2844/2908030 by guest on 28 January 2020

(Dehnen 1998; Skuljan, Hearnshaw & Cottrell 1999; Nordström et al. 2004). Famaey et al. (2005), Famaey, Siebert & Jorissen (2008) and Pompéia et al. (2011) show that although these streams include clusters, after which they are named, and evaporated remnants from these clusters, the majority of stars in these streams are not coeval but include stars of different ages, not necessarily born in the same place nor at the same time. They argue that these streams are dynamical (resonant) in origin, probably related to dynamical perturbations by transient spiral waves (De Simone, Wu & Tremaine 2004), which migrate stars radially to specific regions of the *UV* plane. Stars in a dynamical stream just share a common velocity vector at this particular epoch. These authors further point out the obvious and important point that dynamical streams are kinematically young and so, integrating backwards in a smooth stationary axisymmetric potential, the orbits of the stars belonging to these streams are non-physical. Does this fundamentally invalidate our calculations?

Famaey et al. (2005) assigned probabilities of each star in their sample belonging to different kinematic groups. They found that stars not belonging to dynamical streams (young giants and the smooth background) make up the majority (70 per cent) of their sample. Seabroke et al. (2008)'s fig. 10 illustrates that the majority of Famaey et al. (2005)'s stars are within ±250 pc of the Galactic plane, with the distribution centred on the Galactic plane. Our RAVE sample of F–G dwarfs shows similar line-of-sight distances from the Sun to Famaey et al. (2005)'s K–M giants (200–400 pc). However, Siebert et al. (2011)'s fig. 15 shows that RAVE stars are selected to avoid the Galactic plane ($|b| > 10^\circ$). This means our RAVE sample will include stars further from the Galactic plane than the Famaey et al. (2005) sample. Dynamical perturbations by transient spiral waves are strongest closest to the Galactic plane, so there will be fewer dynamical-stream stars in our RAVE sample. While we could in principle assign our stars to different kinematic groups compared with Famaey et al. (2005), it is probable that our sample has more than the local 70 per cent of stars that have orbital parameters that can be determined adequately from the static Milky Way disc potential and are not influenced by transient spiral waves. Famaey et al. (2005)'s space velocities are also much more accurate than our RAVE values so, considering all factors, we have not attempted to remove dynamical-stream stars from our sample. Contamination is unlikely to affect our statistical results.

To determine a possible orbit, we first perform test-particle integration in a Milky Way potential, which consists of a logarithmic halo of the form

$$\Phi_{\rm halo}(r) = v_0^2 \ln\left(1 + \frac{r^2}{d^2}\right), \tag{2}$$

with $v_0 = 186\,{\rm km\,s^{-1}}$ and $d = 12\,{\rm kpc}$. The disc is represented by a Miyamoto–Nagai potential:

$$\Phi_{\rm disc}(R, z) = -\frac{GM_{\rm d}}{\sqrt{R^2 + \left(a_{\rm d} + \sqrt{z^2 + b_{\rm d}^2}\right)^2}}, \tag{3}$$

with $M_{\rm d} = 10^{11}\,{\rm M}_\odot$, $a_{\rm d} = 6.5\,{\rm kpc}$ and $b_{\rm d} = 0.26\,{\rm kpc}$. Finally, the bulge is modelled as a Hernquist potential:

$$\Phi_{\rm bulge}(r) = -\frac{GM_{\rm b}}{r + c}, \tag{4}$$

using $M_{\rm b} = 3.4 \times 10^{10}\,{\rm M}_\odot$ and $c = 0.7\,{\rm kpc}$. The superposition of these components gives quite a good representation of the Milky Way. The circular speed at the solar radius is $\sim$220 km s$^{-1}$, $P_{\rm LSR} = 2.18 \times 10^8$ yr is the orbital period of the LSR and $V_{\rm c} = 222.5\,{\rm km\,s^{-1}}$ denotes the circular rotational velocity at the solar Galactocentric distance, $R_0 = 8\,{\rm kpc}$.

For our analysis of gradients, we are interested in the mean radial Galactocentric distance ($R_{\rm m}$) as a function of the stellar population and the orbital shape. Wilson et al. (2011) have analysed the radial orbital eccentricities of a RAVE sample of thick-disc stars, to test thick-disc formation models. Here we focus on possible local gradients, so instead we consider the *vertical* orbital eccentricity, $e_{\rm v}$. $R_{\rm m}$ is defined as the arithmetic mean of the final perigalactic ($R_{\rm p}$) and apogalactic ($R_{\rm a}$) distances, whereas $e_{\rm v}$ is defined as follows:

$$e_{\rm v} = \frac{(|Z_{\rm max}| + |Z_{\rm min}|)}{R_{\rm m}}, \tag{5}$$

where $R_{\rm m} = (R_{\rm a} + R_{\rm p})/2$ (Pauli 2005). Due to $z$-excursions, $R_{\rm p}$ and $R_{\rm a}$ can vary; however, this variation is no more than 5 per cent.

## 4 POPULATION ANALYSIS

### 4.1 Classification using space motions

The procedure of Bensby, Feltzing & Lundström (2003) and Bensby et al. (2005) was used to separate sample stars into different populations. This kinematic methodology assumes that Galactic space velocities for the thin disc (*D*), thick disc (*TD*) and stellar halo (*H*) with respect to the LSR have Gaussian distributions as follows:

$$f(U,\ V,\ W) = k \times \exp\left(-\frac{U_{\rm LSR}^2}{2\sigma_{U_{\rm LSR}}^2} - \frac{(V_{\rm LSR} - V_{\rm asym})^2}{2\sigma_{V_{\rm LSR}}^2} - \frac{W_{\rm LSR}^2}{2\sigma_{W_{\rm LSR}}^2}\right), \tag{6}$$

where

$$k = \frac{1}{(2\pi)^{3/2}\sigma_{U_{\rm LSR}}\sigma_{V_{\rm LSR}}\sigma_{W_{\rm LSR}}} \tag{7}$$

normalizes the expression. For consistency with other analyses, $\sigma_{U_{\rm LSR}}$, $\sigma_{V_{\rm LSR}}$ and $\sigma_{W_{\rm LSR}}$ were adopted as the characteristic velocity dispersions: 35, 20 and 16 km s$^{-1}$ for the thin disc (*D*), 67, 38 and 35 km s$^{-1}$ for the thick disc (*TD*) and 160, 90 and 90 km s$^{-1}$ for the halo (*H*), respectively (Bensby et al. 2003). $V_{\rm asym}$ is the asymmetric drift: −15, −46 and −220 km s$^{-1}$ for the thin disc, thick disc and halo, respectively. LSR velocities were taken from Coşkunoğlu et al. (2011) and these values are $(U, V, W)_{\rm LSR} = (8.83 \pm 0.24, 14.19 \pm 0.34, 6.57 \pm 0.21)\,{\rm km\,s^{-1}}$.

The probability of a star of being 'a member' of a given population is defined as the ratio of the $f(U, V, W)$ distribution functions times the ratio of the local space densities for two populations. Thus,

$$TD/D = \frac{X_{\rm TD}}{X_{\rm D}} \times \frac{f_{\rm TD}}{f_{\rm D}}, \qquad TD/H = \frac{X_{\rm TD}}{X_{\rm H}} \times \frac{f_{\rm TD}}{f_{\rm H}}, \tag{8}$$

are the probabilities for a star being classified as a thick-disc star relative to it being classified as a thin-disc star or a halo star, respectively. $X_{\rm D}$, $X_{\rm TD}$ and $X_{\rm H}$ are the local space densities for thin disc, thick disc and halo, i.e. 0.94, 0.06 and 0.0015, respectively (Robin et al. 1996; Buser, Rong & Karaali 1999). We followed the argument of Bensby et al. (2005) and separated the sample stars into four categories: $TD/D \leq 0.1$ (high-probability thin-disc stars), $0.1 < TD/D \leq 1$ (low-probability thin-disc stars), $1 < TD/D \leq 10$ (low-probability thick-disc stars) and $TD/D > 10$ (high-probability thick-disc stars). Fig. 1 shows the *U*–*V* and *W*–*V* diagrams as a function of spectral types and population types defined by using Bensby et al. (2003)'s criteria. It is evident from Fig. 1 that the kinematic population assignments are strongly affected by space-motion uncertainties.

Downloaded from https://academic.oup.com/mnras/article-abstract/419/4/2844/2908030 by guest on 28 January 2020

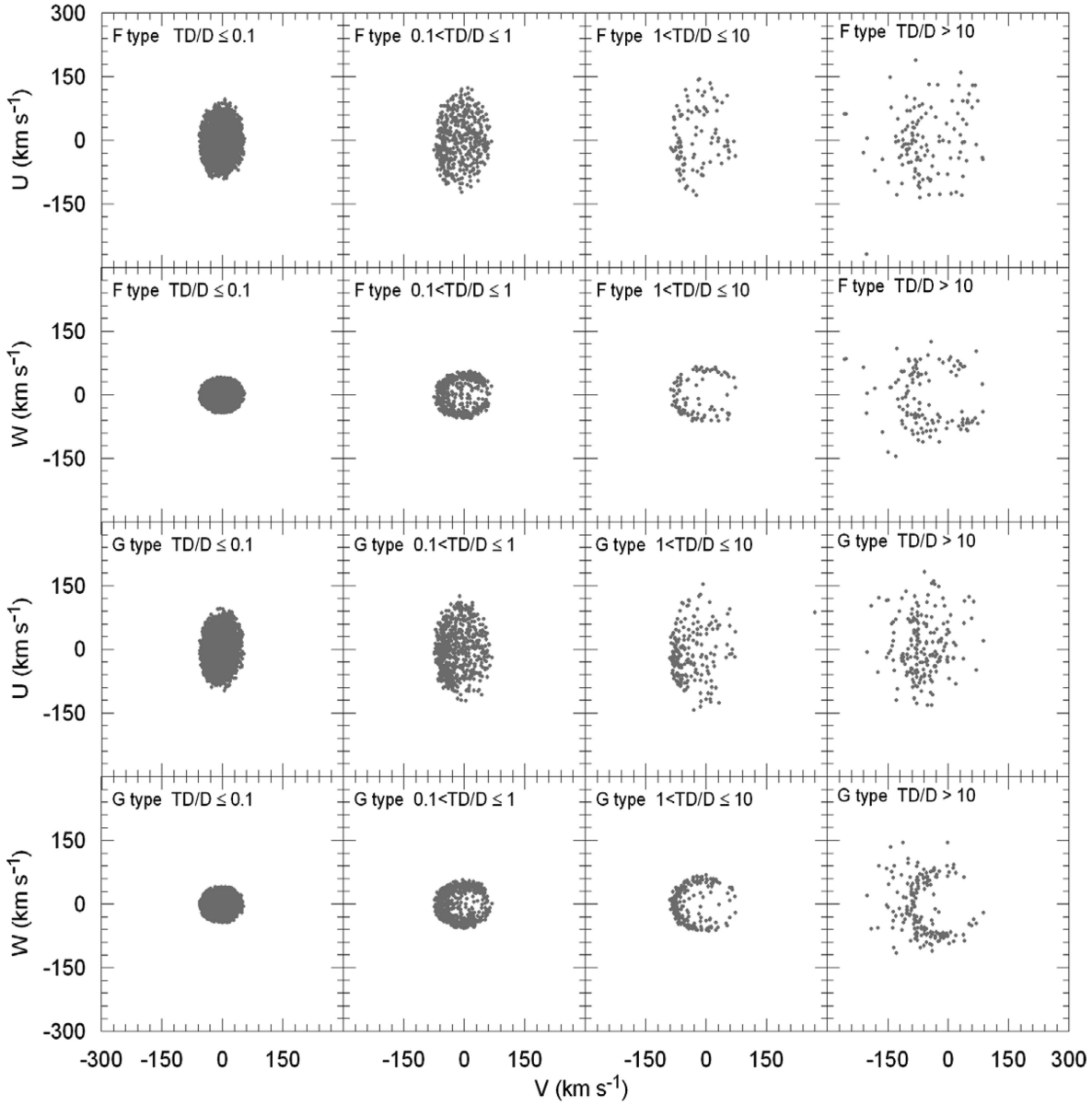


**Figure 1.** *U*–*V* and *W*–*V* diagrams of F- and G-type stars applying Bensby et al. (2003)'s population classification criteria. It is apparent that space-motion uncertainties remain significant, even for this nearby sample.

**Table 1.** Population frequency distribution of sample stars according to Bensby et al. (2003)'s kinematical criteria. *TD*/*D* ranges are explained in the text.

| | Number of stars | | | | |
|---|---|---|---|---|---|
| Spectral type | $TD/D \leq 0.1$ | $0.1 < TD/D \leq 1$ | $1 < TD/D \leq 10$ | $TD/D > 10$ | Total |
| F & G type stars | 15270 | 1142 | 287 | 309 | 17008 |
| F type stars | 9566 | 484 | 97 | 124 | 10271 |
| G type stars | 5704 | 658 | 190 | 185 | 6737 |

Using Fig. 1, 15 270 and 1142 stars of the sample were classified as high- and low-probability thin-disc stars, respectively, whereas 287 and 309 stars are low- and high-probability thick-disc stars (Table 1). The relative number of high-probability thick- and thin-disc stars (2 per cent) is evidently very much lower than the number expected, especially for a sample biased towards intermediate Galactic latitudes.

### 4.2 Classification using stellar vertical orbital shape

Both radial and vertical orbital eccentricities contain valuable information: here we consider the vertical orbit shape. Vertical orbital eccentricities were calculated, as described above, from numerically integrated orbits. We term this the dynamical method. Fig. 2 shows that the distribution functions of $e_v$ for F- and G-type stars,

© 2011 The Authors, MNRAS **419,** 2844–2854
Monthly Notices of the Royal Astronomical Society © 2011 RAS

Downloaded from https://academic.oup.com/mnras/article-abstract/419/4/2844/2908030 by guest on 28 January 2020

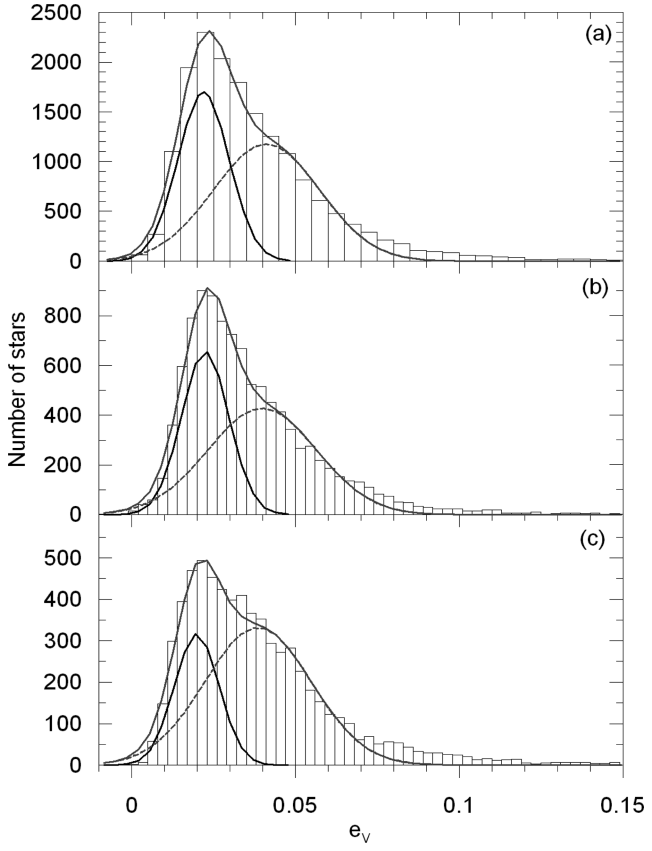


**Figure 2.** Three vertical eccentricity distributions, for (a) F- and G- type stars, (b) F-type stars and (c) G-type stars.

considered separately or in total, are not consistent with their comprising a single Gaussian distribution. A two-Gaussian model, however, does provide an acceptable fit. Hence, we separated our sample into three categories – stars with $e_v \leq 0.04$, $0.04 < e_v \leq 0.1$ and $e_v > 0.1$ – for each spectral type and fitted their metallicities to their mean radial distances ($R_m$) in order to investigate the presence of a metallicity gradient for RAVE stars. We provide the full version of Table 2 electronically (see Supporting Information), which includes stellar parameters from RAVE DR3, calculated kinematical and dynamical parameters and stellar population for the entire sample. The categories and the number of stars corresponding to these categories are given in Table 3.

## 5 RESULTS

### 5.1 Metallicity gradients from the kinematical population-assignment method

The metallicity distribution functions of our final sample, divided into two spectral types, are shown in Fig. 3. We note these are RAVE DR3 metallicities [*M*/H] and not standard [Fe/H] values. As seen from the figure, the metallicity distribution extends from −0.7 to +1 dex. We now consider the metallicities as a function of the mean orbital Galactocentric radial distance ($R_m$) for each different population, i.e. for F- and G-type stars, and test for the presence of a metallicity gradient for each population. We fitted the distributions to linear equations, the gradient of which is any metallicity gradient, $d[M/H]/dR_m$. The results are shown in Fig. 4. The metallicity gradients in all panels of Fig. 4 are either small or consistent with zero. The best-determined values are for high-probability thin-disc stars, where the gradient is $d[M/H]/dR_m$ is $-0.043 \pm 0.005$ dex kpc$^{-1}$ for F-type stars and $-0.033 \pm 0.007$ dex kpc$^{-1}$ for G-type stars (Table 4). Interestingly, the metallicity gradient for high-probability thick-disc stars is consistent with zero. However, we treat this value with caution, for the number of stars is only 124 and 185 for F- and G-types, respectively, for this population, and Fig. 1 reminds us that space-motion errors are important. Wilson et al. (2011) discusses RAVE thick-disc stars in more detail.

### 5.2 Metallicity gradients from the dynamical population-assignment method

We divide the data into three bins of vertical orbital eccentricity and test for any dependence of metallicity on mean radial Galactocentric distance, $R_m$, again using linear fits. The results are presented in Fig. 5 and Table 4. We detect a significant metallicity gradient for high-probability F-type thin-disc stars of $d[M/H]/dR_m = -0.051 \pm 0.005$ dex kpc$^{-1}$. For G-type stars the metallicity gradients are rather lower, being consistent with zero (Fig. 5 and Table 4).

These results are consistent with there being somewhat steeper abundance gradients in younger stars than in older. We test that further in the next section.

### 5.3 Metallicity limitation for metal-rich stars

The RAVE pipeline derives metallicity, as any other parameter, using a penalized $\chi^2$ technique by finding an optimal match between the observed spectrum and a spectrum constructed from a library of precomputed synthetic spectra. The metallicity results match if a similar analysis method is used. The results of the analysis using an independent $\chi^2$ procedure (Munari et al. 2005) yield metallicities that are entirely consistent with the RAVE pipeline results, i.e. a mean offset of $0.04 \pm 0.02$ dex and a standard deviation of 0.17 dex. RAVE metallicities as derived from the RAVE pipeline are part of a self-consistent native RAVE system of stellar parameters, which are tied to a $\chi^2$ analysis using a library of Kurucz template spectra.

However, other spectral methods that derive metallicities from the strengths of individual spectral lines and not from a $\chi^2$ match of synthetic and observed spectra do not yield results very consistent with those from the RAVE pipeline. As usual, calibration of an internal abundance scale on to standard external systems requires special consideration. One can see the following trends in a comparison of metallicities derived by other methods and the RAVE pipeline.

(i) The difference between RAVE and reference metallicity increases with an increased $\alpha$-enhancement, in the sense that RAVE values become too metal-poor.

(ii) The difference is larger at lower metallicities.

(iii) The difference is larger for giants than for main-sequence stars, though the variation is much weaker than $\alpha$-enhancement or metallicity.

(iv) The difference does not depend on temperature.

In Zwitter et al. (2008), the RAVE metallicities ([*m*/H]) derived by the $\chi^2$ method were calibrated to the metallicities ([*M*/H]), which are in line with the metallicity system of the datasets *in situ*, such as those appearing in the Asiago Observatory and Soubiran & Girard (2005) catalogues. The final calibration is as follows:

$$[M/H] = 0.938[m/H] + 0.767[\alpha/Fe] - 0.064 \log g + 0.404. \quad (9)$$

Downloaded from https://academic.oup.com/mnras/article-abstract/419/4/2844/2908030 by guest on 28 January 2020

**Table 2.** Stellar atmospheric parameters, astrometric, kinematic and dynamic data for the whole sample. (1) ID, (2) designation, (3)–(4) equatorial coordinates in degrees, (5) $T_{\rm eff}$ in K, (6) $\log g$ (cm s$^2$), (7) calibrated metallicity [$M$/H] (dex), (8)–(9) proper-motion components in mas yr$^{-1}$, (10) $d$ in kpc, (11) heliocentric radial velocity in km s$^{-1}$, (12)–(17) Galactic space-velocity components and their respective errors in km s$^{-1}$, (18)–(19) perigalactic and apogalactic distance in kpc, (20)–(21) minimum and maximum distance from the Galactic plane in kpc, (22) *TD/D* ratio as mentioned in the text. This is a sample of the full table, which is available with the electronic version of the article (see Supporting Information).

| (1) ID | (2) Designation | (3) $\alpha$ | (4) $\delta$ | (5) $T_{\rm eff}$ | (6) $\log g$ | (7) [$M$/H] | (8) $\mu_\alpha \cos\delta$ | (9) $\mu_\delta$ | (10) $d$ | (11) $\gamma$ | (12) $U_{\rm LSR}$ | (13) $U_{\rm err}$ | (14) $V_{\rm LSR}$ | (15) $V_{\rm err}$ | (16) $W_{\rm LSR}$ | (17) $W_{\rm err}$ | (18) $d_{\rm per}$ | (19) $d_{\rm apo}$ | (20) $z_{\rm min}$ | (21) $z_{\rm max}$ | (22) *TD/D* |
|---|---|---|---|---|---|---|---|---|---|---|---|---|---|---|---|---|---|---|---|---|---|
| 1 | J000018.6–094053 | 0.077375 | −9.681528 | 6306 | 4.16 | 0.10 | −1.60 | −7.50 | 0.345 | −5.4 | 13.34 | 3.40 | 3.03 | 3.32 | 8.27 | 1.75 | 7.678 | 8.475 | −0.351 | 0.351 | 0.006 |
| 2 | J000020.3–520757 | 0.084458 | −52.132528 | 5761 | 4.06 | 0.06 | −12.00 | 5.10 | 0.289 | 30.3 | 33.37 | 6.13 | 18.20 | 6.11 | −20.21 | 2.97 | 7.474 | 9.708 | −0.386 | 0.394 | 0.018 |
| 3 | J000022.6–265716 | 0.094250 | −26.954694 | 6080 | 4.50 | 0.49 | −6.10 | 2.60 | 0.498 | 12.6 | 19.15 | 10.99 | 26.83 | 11.10 | −3.00 | 3.75 | 7.799 | 10.091 | −0.566 | 0.564 | 0.012 |
| 4 | J000025.9–373329 | 0.107750 | −37.558056 | 6590 | 4.74 | −0.08 | −6.70 | 5.20 | 0.380 | 23.1 | 21.68 | 2.85 | 25.91 | 3.55 | −15.08 | 1.40 | 7.747 | 10.007 | −0.473 | 0.474 | 0.016 |
| 5 | J000026.3–394148 | 0.109500 | −39.696861 | 6693 | 4.19 | −0.11 | −21.20 | −11.80 | 0.259 | 21.8 | 43.75 | 3.26 | 10.29 | 1.72 | −6.41 | 1.20 | 7.154 | 9.591 | −0.286 | 0.285 | 0.011 |
| 6 | J000026.4–671654 | 0.110125 | −67.281917 | 5773 | 4.46 | 0.06 | −15.50 | −12.10 | 0.158 | 26.1 | 34.14 | 1.95 | −0.85 | 1.61 | −5.35 | 2.03 | 7.023 | 8.804 | −0.135 | 0.135 | 0.007 |
| 7 | J000029.4–402006 | 0.122500 | −40.335083 | 5891 | 4.16 | −0.16 | −2.00 | −13.10 | 0.133 | 39.6 | 24.15 | 0.97 | 2.75 | 1.09 | −29.43 | 0.74 | 7.410 | 8.719 | −0.367 | 0.375 | 0.022 |
| 8 | J000031.4–592708 | 0.130667 | −59.452250 | 6342 | 4.53 | 0.22 | 8.50 | −13.10 | 0.334 | 6.7 | 9.15 | 7.67 | −11.75 | 7.94 | 8.91 | 5.03 | 6.986 | 7.958 | −0.302 | 0.304 | 0.007 |
| 9 | J000033.7–483342 | 0.140542 | −48.561889 | 6489 | 4.10 | −0.06 | −20.10 | −2.60 | 0.345 | 23.0 | 48.53 | 4.43 | 19.22 | 3.65 | −6.71 | 2.31 | 7.201 | 10.201 | −0.374 | 0.374 | 0.016 |
| 10 | J000034.3–372147 | 0.143042 | −37.363250 | 5893 | 4.10 | −0.22 | −17.40 | −5.20 | 0.121 | −9.3 | 16.48 | 1.22 | 16.17 | 0.62 | 17.88 | 1.01 | 7.794 | 9.218 | −0.254 | 0.254 | 0.012 |
| 11 | J000039.2–505940 | 0.163500 | −50.994639 | 5746 | 4.06 | 0.16 | 17.20 | 0.50 | 0.462 | −1.6 | −21.80 | 11.22 | −1.94 | 11.08 | 0.09 | 5.21 | 7.341 | 8.278 | −0.429 | 0.429 | 0.006 |
| 12 | J000042.6–495123 | 0.177333 | −49.856556 | 5771 | 4.20 | 0.01 | 41.20 | −43.50 | 0.236 | −1.3 | −13.11 | 3.14 | −48.33 | 6.53 | 16.61 | 1.93 | 5.115 | 7.944 | −0.300 | 0.298 | 0.062 |
| 13 | J000042.8–254548 | 0.178542 | −25.763528 | 6742 | 4.67 | 0.53 | −28.00 | −14.00 | 0.511 | −4.3 | 81.15 | 9.91 | 13.38 | 5.39 | 22.78 | 2.43 | 6.586 | 11.286 | −0.732 | 0.732 | 0.102 |
| 14 | J000100.5–363932 | 0.251917 | −36.659028 | 5647 | 4.52 | 0.07 | −11.80 | −17.00 | 0.348 | 18.8 | 42.51 | 8.05 | −3.62 | 7.91 | −3.71 | 2.33 | 6.793 | 8.983 | −0.364 | 0.364 | 0.009 |
| 15 | J000105.4–540845 | 0.272333 | −54.146083 | 5720 | 4.05 | 0.05 | 16.10 | −0.80 | 0.248 | 6.5 | −3.13 | 3.78 | 2.36 | 3.59 | −2.53 | 2.02 | 7.909 | 7.973 | −0.219 | 0.219 | 0.005 |
| 16 | J000107.9–412207 | 0.282917 | −41.368861 | 6461 | 4.49 | 0.31 | −0.60 | 4.70 | 0.342 | 13.6 | 11.31 | 2.36 | 19.14 | 2.51 | −8.10 | 2.86 | 7.830 | 9.302 | −0.369 | 0.370 | 0.008 |
| 17 | J000108.8–493742 | 0.286542 | −49.628556 | 5857 | 4.68 | 0.07 | −35.10 | −27.40 | 0.282 | −1.4 | 64.18 | 6.12 | 3.55 | 3.18 | 30.23 | 3.00 | 6.592 | 10.002 | −0.530 | 0.530 | 0.077 |
| 18 | J000124.0–345502 | 0.350125 | −34.917417 | 5616 | 4.85 | 0.01 | 12.70 | 4.50 | 0.194 | 6.9 | −1.66 | 2.15 | 12.07 | 1.84 | −3.04 | 1.09 | 7.958 | 8.667 | −0.198 | 0.198 | 0.006 |
| 19 | J000129.9–595545 | 0.374667 | −59.929194 | 6413 | 4.45 | −0.28 | 22.70 | 11.80 | 0.254 | −31.3 | −28.82 | 4.29 | 25.28 | 3.33 | 19.72 | 2.45 | 7.722 | 9.991 | −0.370 | 0.370 | 0.023 |
| 20 | J000137.7–701927 | 0.407208 | −70.324222 | 6158 | 4.72 | 0.09 | 23.50 | −28.90 | 0.140 | 25.5 | 12.37 | 1.28 | −20.67 | 2.19 | −2.21 | 1.34 | 6.477 | 8.019 | −0.102 | 0.102 | 0.008 |
| 21 | J000140.8–663745 | 0.419917 | −66.629194 | 5445 | 4.27 | 0.25 | 49.30 | −9.70 | 0.301 | 13.6 | −39.63 | 9.07 | −34.98 | 7.98 | −8.89 | 5.26 | 5.594 | 8.233 | −0.249 | 0.249 | 0.025 |
| 22 | J000142.4–290833 | 0.426542 | −29.142694 | 5696 | 4.03 | −0.30 | 62.60 | −58.80 | 0.173 | −20.0 | −18.33 | 2.59 | −53.51 | 6.65 | 17.43 | 1.40 | 4.875 | 8.013 | −0.273 | 0.273 | 0.108 |
| 23 | J000153.2–783310 | 0.471792 | −78.552917 | 5494 | 4.01 | 0.44 | 12.50 | −2.00 | 0.456 | −30.4 | −20.46 | 11.51 | 17.82 | 10.17 | 23.40 | 10.20 | 7.694 | 9.256 | −0.460 | 0.459 | 0.019 |
| 24 | J000155.8–684858 | 0.482292 | −68.816222 | 6647 | 4.71 | 0.46 | 10.20 | −12.30 | 0.250 | 12.9 | 10.52 | 2.30 | −9.11 | 2.33 | 4.01 | 1.70 | 7.102 | 8.011 | −0.193 | 0.194 | 0.006 |
| 25 | J000159.8–533900 | 0.499125 | −53.650056 | 6170 | 4.28 | 0.24 | −0.70 | −10.70 | 0.570 | 21.6 | 32.46 | 8.38 | −16.69 | 8.43 | 0.17 | 4.44 | 6.403 | 8.277 | −0.519 | 0.520 | 0.009 |
| 26 | J000203.5–353502 | 0.514500 | −35.583917 | 6628 | 4.96 | 0.08 | 41.60 | −12.70 | 0.244 | −18.3 | −31.05 | 4.03 | −20.33 | 4.21 | 17.06 | 1.53 | 6.401 | 8.252 | −0.331 | 0.331 | 0.015 |
| 27 | J000204.0–483953 | 0.516875 | −48.665000 | 6317 | 4.28 | 0.25 | −11.30 | −12.60 | 0.589 | 37.2 | 64.83 | 7.27 | −11.52 | 6.45 | −9.29 | 3.54 | 6.088 | 9.338 | −0.621 | 0.622 | 0.022 |
| 28 | J000207.2–582534 | 0.530167 | −58.426306 | 5624 | 4.13 | 0.31 | 65.80 | −12.60 | 0.276 | 19.7 | −51.15 | 8.28 | −45.87 | 6.88 | −18.27 | 2.96 | 5.035 | 8.387 | −0.313 | 0.313 | 0.107 |
| 29 | J000207.8–355834 | 0.532583 | −35.976222 | 6203 | 4.29 | 0.39 | −1.50 | −24.40 | 0.420 | −1.4 | 32.20 | 6.97 | −28.31 | 6.02 | 15.25 | 2.02 | 5.950 | 8.255 | −0.468 | 0.470 | 0.020 |
| 30 | J000213.6–570608 | 0.556583 | −57.102361 | 6166 | 4.11 | 0.41 | 26.70 | 8.20 | 0.537 | −12.2 | −56.57 | 13.96 | 4.30 | 12.63 | −6.09 | 7.62 | 6.824 | 9.564 | −0.519 | 0.518 | 0.014 |
| 31 | J000220.6–630157 | 0.585792 | −63.032722 | 5231 | 4.15 | 0.12 | −24.40 | 8.60 | 0.281 | 13.0 | 42.44 | 4.39 | 31.34 | 4.28 | −4.33 | 3.22 | 7.451 | 10.799 | −0.273 | 0.271 | 0.023 |
| 32 | J000222.8–245251 | 0.594917 | −24.880861 | 6079 | 4.48 | 0.22 | 38.60 | −26.60 | 0.241 | −28.7 | −20.74 | 2.92 | −36.62 | 4.86 | 24.80 | 1.48 | 5.702 | 8.048 | −0.404 | 0.405 | 0.048 |
| 33 | J000224.1–840559 | 0.600292 | −84.099778 | 6219 | 4.10 | 0.04 | 7.10 | 7.40 | 0.295 | −8.5 | 0.31 | 2.97 | 20.79 | 2.35 | 0.71 | 2.71 | 7.860 | 9.237 | −0.175 | 0.175 | 0.008 |
| 34 | J000227.2–081124 | 0.613167 | −8.190139 | 5672 | 4.46 | 0.27 | −21.80 | −39.80 | 0.285 | −28.5 | 57.48 | 12.76 | −27.14 | 11.04 | 20.78 | 4.89 | 5.757 | 8.980 | −0.383 | 0.380 | 0.051 |
| 35 | J000228.7–405838 | 0.619417 | −40.977444 | 6118 | 4.09 | −0.25 | 85.50 | −2.30 | 0.187 | −38.8 | −66.51 | 6.78 | −17.49 | 3.96 | 29.68 | 1.66 | 6.035 | 9.227 | −0.464 | 0.464 | 0.097 |
| 36 | J000230.7–531342 | 0.627917 | −53.228444 | 6545 | 4.09 | −0.25 | 26.00 | −0.60 | 0.345 | 1.2 | −24.86 | 5.24 | −6.74 | 4.26 | −2.22 | 2.33 | 7.090 | 8.257 | −0.313 | 0.313 | 0.006 |
| 37 | J000232.7–395555 | 0.636417 | −39.932139 | 5987 | 4.06 | −0.10 | 25.10 | −2.50 | 0.321 | 1.1 | −21.95 | 5.31 | −7.01 | 4.94 | −1.02 | 1.71 | 7.148 | 8.212 | −0.314 | 0.313 | 0.006 |
| 38 | J000233.6–531053 | 0.639917 | −53.181444 | 6064 | 4.04 | 0.07 | 33.00 | −20.10 | 0.294 | 11.8 | −15.40 | 3.96 | −34.19 | 5.41 | −0.83 | 2.00 | 5.793 | 7.947 | −0.261 | 0.261 | 0.014 |
| 39 | J000246.2–673717 | 0.692667 | −67.621611 | 5643 | 4.28 | 0.16 | 40.70 | −26.90 | 0.185 | 1.5 | −13.59 | 2.80 | −20.53 | 3.44 | 13.50 | 1.53 | 6.531 | 7.975 | −0.212 | 0.212 | 0.010 |
| 40 | J000255.7–625220 | 0.732125 | −62.872250 | 5954 | 4.61 | −0.07 | −5.10 | −10.80 | 0.119 | −19.5 | 6.45 | 1.28 | 18.97 | 1.24 | 26.08 | 1.02 | 7.917 | 9.267 | −0.348 | 0.347 | 0.022 |
| ... | ... | ... | ... | ... | ... | ... | ... | ... | ... | ... | ... | ... | ... | ... | ... | ... | ... | ... | ... | ... | ... |
| ... | ... | ... | ... | ... | ... | ... | ... | ... | ... | ... | ... | ... | ... | ... | ... | ... | ... | ... | ... | ... | ... |
| ... | ... | ... | ... | ... | ... | ... | ... | ... | ... | ... | ... | ... | ... | ... | ... | ... | ... | ... | ... | ... | ... |

© 2011 The Authors, MNRAS **419,** 2844–2854
Monthly Notices of the Royal Astronomical Society © 2011 RAS

Downloaded from https://academic.oup.com/mnras/article-abstract/419/4/2844/2908030 by guest on 28 January 2020

**Table 3.** Vertical eccentricity frequency distribution of sample stars.

| Spectral type | Number of stars $e_v \leq 0.04$ | $0.04 < e_v \leq 0.1$ | $e_v > 0.1$ | Total |
|---|---|---|---|---|
| F-type stars | 6923 | 3145 | 203 | 10271 |
| G-type stars | 4223 | 2264 | 250 | 6737 |

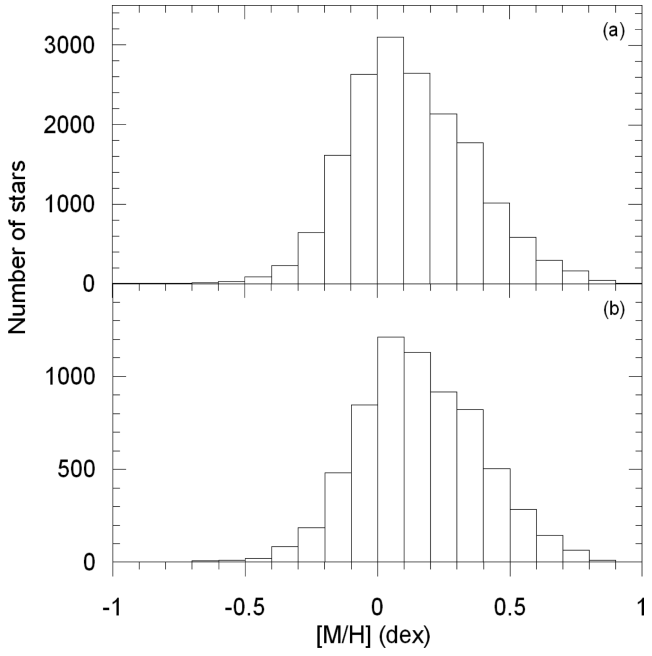


**Figure 3.** Metallicity distributions for (a) F-type and (b) G-type stars.

The classical indicator for the metal abundance is the iron abundance, [Fe/H]. The following relation between the calibrated metallicity and the iron abundance taken from Zwitter et al. (2008) produces a limitation for metal-rich stars:

$$[M/\mathrm{H}] = [\mathrm{Fe/H}] + 0.11[1 \pm (1 - \mathrm{e}^{-3.6|[\mathrm{Fe/H}]+0.55|})], \quad (10)$$

where the plus sign applies for [Fe/H] $< -0.55$ dex and the minus sign otherwise. As the observed upper limit of metal-rich stars is about [Fe/H] $= +0.5$ dex, this is the case for calibrated metallicity as well, i.e. approximately $[M/\mathrm{H}] \leq 0.5$.

### 5.4 Metallicity gradients from blue stars with $[M/\mathrm{H}] \leq +0.5$

Our analyses above (Table 4) show that there are differences between the metallicity gradients estimated from F and G spectral-type stars, in the sense that abundance gradients derived from RAVE F-type stars are steeper than the metallicity gradients from G-type stars. We test this result further by separating the data into two spectral-type subsamples, F0–F3 and F4–G9, and estimating metallicity gradients for these subsamples. The results are shown in Fig. 6. The significant result is that the metallicity gradients for high-probability thin-disc stars (*TD*/*D* $\leq 0.1$ in Table 4) became steeper, i.e. $-0.054 \pm 0.008$ dex kpc$^{-1}$ and $-0.050 \pm 0.015$ dex kpc$^{-1}$ for stars of population type F0–F3 and F4–G9 respectively.

As noted in Section 5.3, the RAVE [*M*/H] distribution does extend to very high abundance values compared with [Fe/H]. In order to test whether the stars with the most extreme [*M*/H] values have systematically unreliable astrophysical parameters, we excluded stars with RAVE [*M*/H] $\geq +0.5$ dex from the sample. We then re-estimated metallicity gradients for the two subsamples cited above, F0–F3 and F4–G9. The result, given in Fig. 7, confirms our apparent trend in the sense that the metallicity gradient estimated from the bluer stars, $-0.065 \pm 0.018$ dex kpc$^{-1}$, is steeper than that obtained from the later spectral-type stars, $-0.025 \pm 0.008$ dex kpc$^{-1}$.

## 6 DISCUSSION AND CONCLUSION

We have used the RAVE DR3 to identify stars classified as dwarfs, further excluding cool stars and those with the most uncertain space motions. We have then obtained a homogeneous sample of dwarfs defined by (1) $4 < \log g \leq 5$, (2) $0.09 < (J-H)_0 \leq 0.39$ and (3) total space-velocity error $S_{\mathrm{err}} \leq 25$ km s$^{-1}$. 10 271 stars of this sample are F-type stars, whereas 6737 of them are G-type stars. For each star we calculated distances and total space motions and integrated the stellar orbit in a Galactic potential to derive both mean Galactocentric distance and stellar orbital shape. We used the calibrated RAVE DR3 metallicities and these mean radial distances to investigate the presence of a radial metallicity gradient, dividing the sample into a variety of subsamples. These subsamples were defined using probabilistic population assignment, considering in turn space motions and stellar Galactic orbital properties – what we term 'kinematic' and 'dynamic' methods. Kinematic properties allowed stars to be separated into four populations, i.e. high-probability thin-disc stars, low-probability thin-disc stars, low-probability thick-disc stars and high-probability thick-disc stars, although only the high-probability thin-disc category retained a sufficiently large sample size for more detailed consideration. In the dynamically defined sample, stars were separated into three subsamples according to their vertical orbital eccentricity, i.e. $e_v \leq 0.04$, $0.04 < e_v \leq 0.10$ and $e_v > 0.10$.

In all cases, we derive significant metallicity gradients for the samples that are *statistically* dominated by the youngest thin-disc stars. We derive significant and marginally shallower gradients for samples that are *statistically* dominated by somewhat older thin-disc stars. We do not detect any gradient in the very small samples of stars categorized as thick-disc. The accuracy and resulting sample size of our thick-disc population assignments is too poor for any robust statements to be made.

Our radial metallicity gradients for high-probability thin-disc stars, defined using either of our two population-classification methods (*TD*/*D* $\leq 0.1$ and $e_v \leq 0.04$ in Table 4), can be compared with values in the literature. Our F-star gradient is $-0.043 \pm 0.005$ dex kpc$^{-1}$. This is somewhat less than the $\mathrm{d[Fe/H]/d}R_{\mathrm{G}} = -0.06 \pm 0.01$ dex kpc$^{-1}$ obtained for young stars (Cepheids: Luck et al. 2011) but is consistent with the thin-disc radial metallicity gradient found by Karataş & Klement (2012) using earlier RAVE data. Karataş & Klement (2012) considered RAVE DR2 data, combining all spectral types and using the RAVE 'calibrated' metallicity scale to derive $\mathrm{d}[M/\mathrm{H}]/\mathrm{d}R = -0.04$ dex kpc$^{-1}$. Any difference between the RAVE and Cepheid gradients may be due to calibration differences. Our thin-disc G-star sample defined using our kinematic approach, *TD*/*D* $\leq 0.1$, produces a gradient ($-0.033 \pm 0.005$ dex kpc$^{-1}$) that is also consistent with the Karataş & Klement (2012) value.

When we define our F- and G-star samples using our orbital shape (dynamic) definition $e_v \leq 0.04$, the resulting abundance gradients ($-0.051 \pm 0.005$ and $-0.020 \pm 0.006$ dex kpc$^{-1}$) agree less well with the Karataş & Klement (2012) value. Interestingly, they are closer to the value derived from RAVE DR2 data using the RAVE DR2 calibrated [*M*/H] ($-0.04$ dex kpc$^{-1}$) than the uncalibrated [*M*/H] ($-0.07$ dex kpc$^{-1}$). The differences between the values derived from the RAVE calibrated [*M*/H] are partly due to

Downloaded from https://academic.oup.com/mnras/article-abstract/419/4/2844/2908030 by guest on 28 January 2020

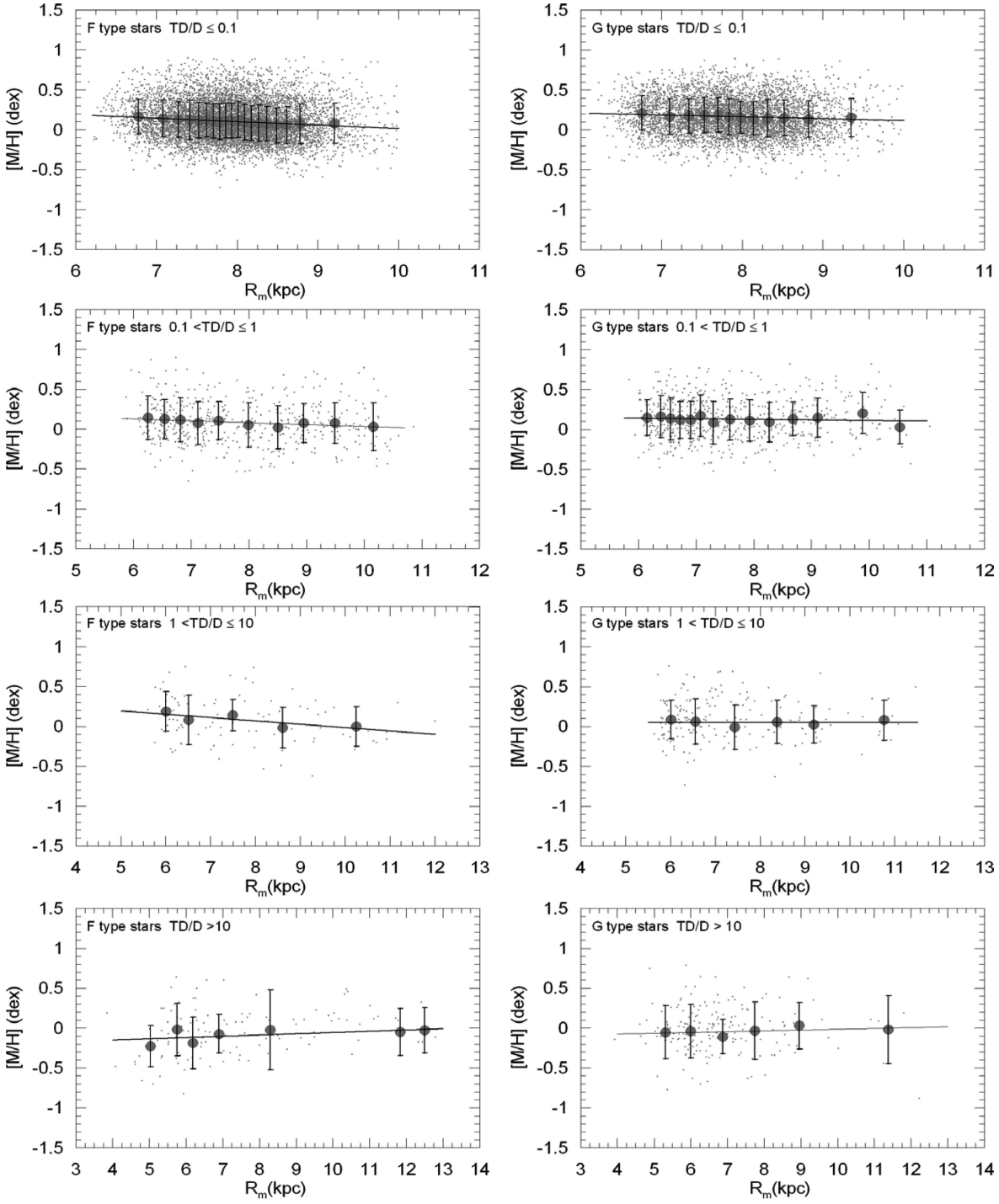


**Figure 4.** $R_{\rm m}$–[$M$/H] diagrams for sample stars as a function of spectral types and populations.

improved statistics, RAVE DR3 having ≈1.5 times more stars than does DR2, but we also warn that RAVE metallicities still need to be calibrated robustly on to a [Fe/H] metallicity scale.

The radial iron gradient for thin-disc stars (4 < age < 6 Gyr) found by Nordström et al. (2004) is $-0.099 \pm 0.011$ dex kpc$^{-1}$. The chemical evolution model of Schönrich & Binney (2009) was tuned to provide an excellent fit to this gradient. In the model, the gradient is caused by radial migration of stars and flow of gas through the disc. This gradient is at least a factor of 2 steeper than our values, presented in Table 3. However, as discussed in Section 3, the RAVE stars of our sample are further from the Galactic plane than the Nordström et al. (2004) stars, so vertical abundance gradients may – or may not – be an additional parameter. At face value, the amplitude of time-dependent effects in models such as that of Schönrich & Binney (2009) may need to be retuned to have a smaller effect for stars further from the plane than Nordström et al. (2004)'s sample, because radial migration of stars and flow of gas through the disc appears to be less effective further from the plane.

The steepest metallicity gradient that we measure, i.e. d[$M$/H]/d$R_{\rm m}$ = $-0.051 \pm 0.005$ dex kpc$^{-1}$, corresponds to the

Downloaded from https://academic.oup.com/mnras/article-abstract/419/4/2844/2908030 by guest on 28 January 2020

**Table 4.** Radial metallicity gradients for F- and G-type stars evaluated from kinematical and dynamical data. Ranges of *TD*/*D* and $e_v$ are explained in the text.

| Population type | F-type stars d[*M*/H]/d$R_m$ (dex kpc$^{-1}$) | Sample size | G-type stars d[*M*/H]/d$R_m$ (dex kpc$^{-1}$) | Sample size |
|---|---|---|---|---|
| $TD/D \leq 0.1$ | $-0.043 \pm 0.005$ | 9566 | $-0.033 \pm 0.007$ | 5704 |
| $0.1 < TD/D \leq 1$ | $-0.024 \pm 0.007$ | 484 | $-0.007 \pm 0.009$ | 658 |
| $1 < TD/D \leq 10$ | $-0.042 \pm 0.017$ | 97 | $0.000 \pm 0.010$ | 190 |
| $TD/D > 10$ | $0.016 \pm 0.011$ | 124 | $0.010 \pm 0.009$ | 185 |
| $e_v \leq 0.04$ | $-0.051 \pm 0.005$ | 6923 | $-0.020 \pm 0.006$ | 4223 |
| $0.04 < e_v \leq 0.1$ | $-0.020 \pm 0.005$ | 3145 | $-0.004 \pm 0.005$ | 2264 |
| $e_v > 0.1$ | $0.016 \pm 0.012$ | 203 | $0.037 \pm 0.016$ | 250 |

subsample of F-type stars defined using orbital shape with eccentricities $e_v \leq 0.04$. The number of stars in this interval is 6923 (67 per cent of the whole sample). It is interesting to note that this value not only is consistent with Cepheid values but also agrees with the value ($-0.050$ dex kpc$^{-1}$) predicted by Rahimi et al. (2011) from their cosmologically simulated galaxy for 'intermediate' disc stars ($7 <$ age $< 10$ Gyr). In their model, negative radial metallicity gradients are due to inside-out formation of the disc. Our stellar sample is, however, biased toward very much lower ages than those modelled by Rahimi et al. (2011).

Although our samples are small and uncertainties large, we do not detect any significant abundance gradient in thick-disc stars using either definition. Our thick-disc radial best-fitting metallicity gradients ($TD/D > 10$ and $e_v > 0.1$ in Table 4) are, however, (marginally significantly) shallower than our gradients for thin-disc stars. The radial iron gradient for thick-disc stars (age $> 10$ Gyr) found by Nordström et al. (2004) is $+0.028 \pm 0.036$ dex kpc$^{-1}$. Our values are closer to the $+0.01 \pm 0.04$ dex kpc$^{-1}$ found by Ruchti et al. (2011) for a metal-poor thick disc. Interestingly these values agree with the chemical evolution models of Chiappini, Matteucci & Gratton (1997) and Chiappini, Matteucci & Romano (2001) ($+0.01$–$0.03$ dex kpc$^{-1}$). These models decompose the disc into radial annuli that exchange neither gas nor stars. Thick-disc stars

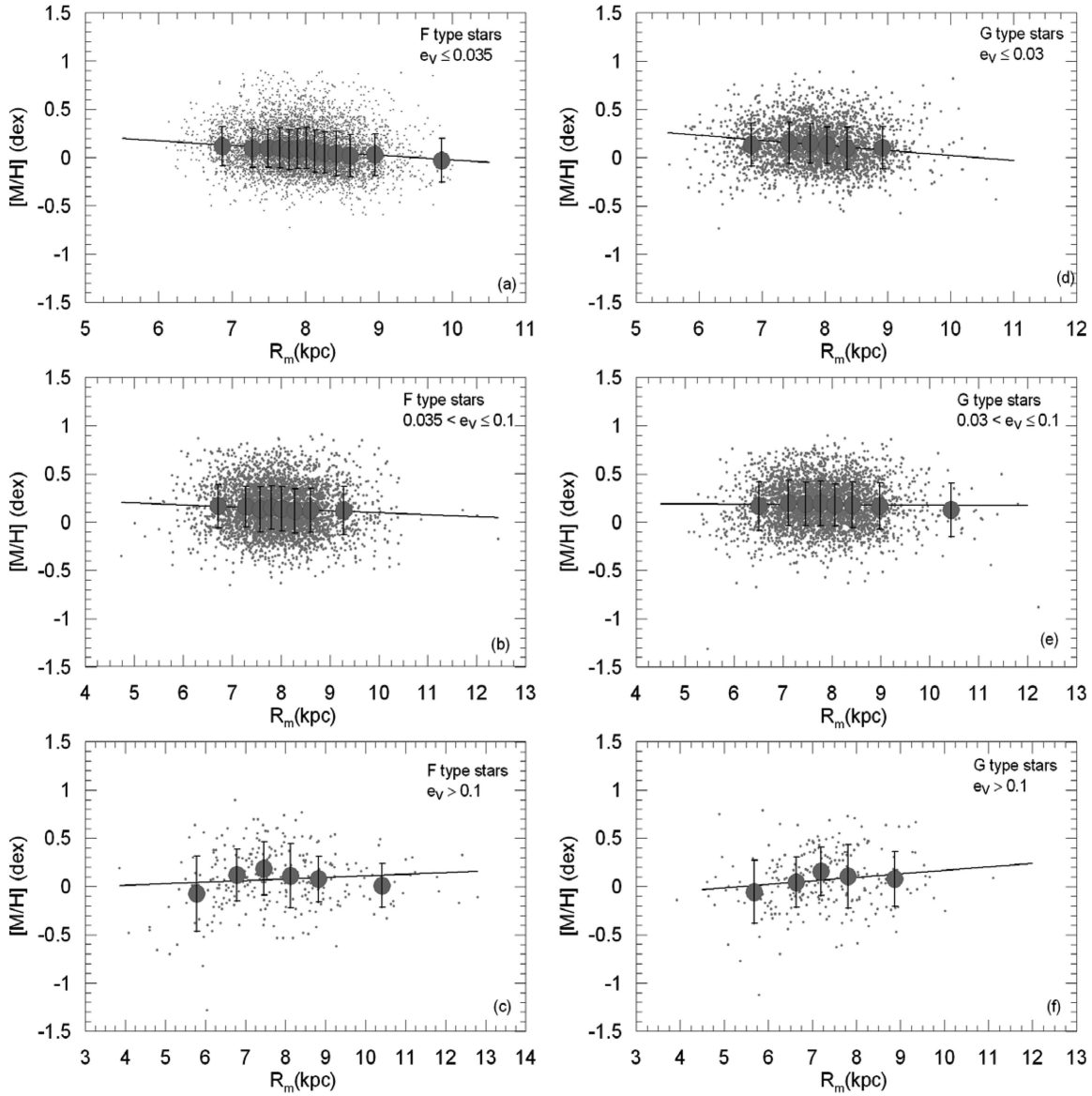


**Figure 5.** $R_m$–[*M*/H] diagrams for sample stars as a function of spectral type and vertical orbital eccentricity.

Downloaded from https://academic.oup.com/mnras/article-abstract/419/4/2844/2908030 by guest on 28 January 2020

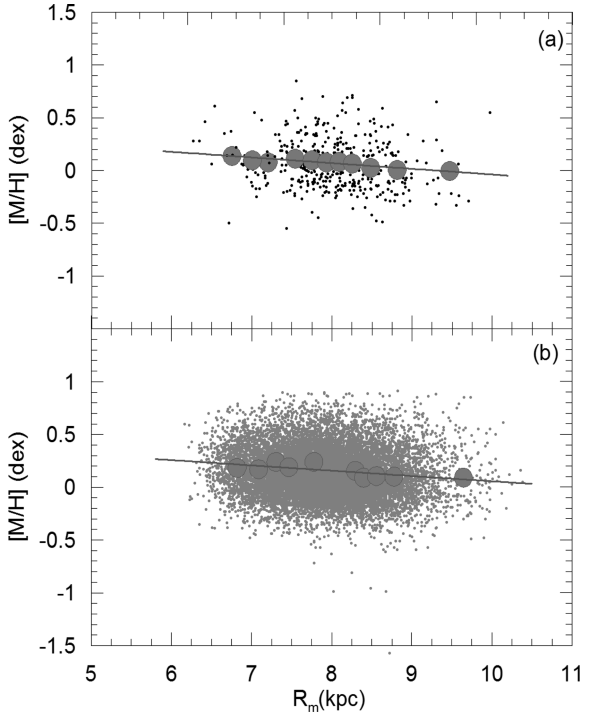


**Figure 6.** $R_{\rm m}$–[$M$/H] diagrams for two subsamples: (a) F0–F3 and (b) F4–G9 spectral types.

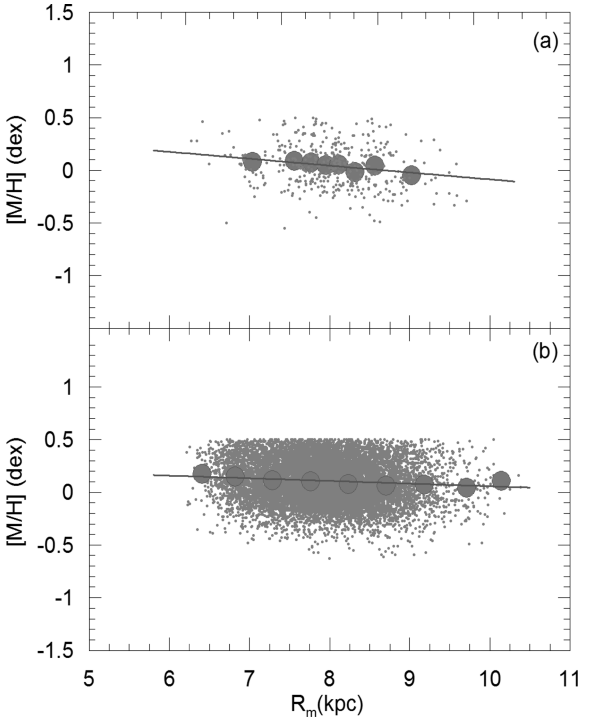


**Figure 7.** $R_{\rm m}$–[$M$/H] diagrams for the same subsamples as in Fig. 6, but with metallicity restriction [$M$/H] $< +0.5$ dex. This selection leads to a steeper metallicity gradient for early spectral-type stars (panel a) and a flatter gradient for later spectral-type stars (panel b).

are, on average, further from the Galactic plane than thin-disc stars and so should be relatively independent of radial mixing (unless radial mixing actually evolves a thin-disc star into a thick-disc star, as suggested by Schönrich & Binney 2009). However, within our large errors, thick-disc stars show no radial gradient at all. This trend is different to that seen in the thin disc, suggesting that these stars do not share the same origin as the thin disc.

Metallicity gradients that we have estimated from F-type stars are steeper than those obtained from G-type stars for a given population (Table 4). Given our sample size, the only robust metallicity gradients we determine are $-0.043 \pm 0.005$ dex kpc$^{-1}$ and $-0.051 \pm 0.005$ dex kpc$^{-1}$ respectively, for stars classified as high-probability thin-disc, i.e. for population types labelled with $TD/D \leq 0.1$ and $e_{\rm v} \leq 0.04$. Separation of the sample into two colour subsamples, F0–F3 and F4–G9 here, provides a steeper metallicity gradient of $-0.065 \pm 0.015$ dex kpc$^{-1}$ for the earlier spectral-type stars. Other subsamples from the RAVE DR3 dwarf sample are very small in number and have relatively large uncertainties. The RAVE DR3 dwarf star sample probes stars with orbits with mean Galactocentric radii within 3 kpc of the solar Galactocentric radius. Stars with spectral types F0–F3, which provide the steeper metallicity gradient of $-0.065 \pm 0.015$ dex kpc$^{-1}$, make up only 3 per cent of the F- and G-type stars with [$M$/H] $< 0.5$ dex.

From our analysis, we conclude that the RAVE DR3 data may be described as two different subsamples, i.e. a thin-disc sample biased toward low ages with a detected metallicity gradient and a thin-disc sample biased to somewhat higher ages in which we do not detect any metallicity gradient.

## ACKNOWLEDGMENTS

We thank the referee Dr B. Barbuy for her comments and suggestions. This work has been supported in part by the Scientific and Technological Research Council (TÜBİTAK) 108T613. GMS is funded by the UK VEGA *Gaia* Data Flow System grant.

This publication makes use of data products from the Two-Micron All-Sky Survey, which is a joint project of the University of Massachusetts and the Infrared Processing and Analysis Center/California Institute of Technology, funded by the National Aeronautics and Space Administration and the National Science Foundation. This research has made use of SIMBAD, NASA's Astrophysics Data System Bibliographic Services and the NASA/IPAC ExtraGalactic Database (NED), which is operated by the Jet Propulsion Laboratory, California Institute of Technology, under contract with the National Aeronautics and Space Administration.

## REFERENCES

Ak S., Bilir S., Karaali S., Buser R., 2007a, Astron. Nachr., 328, 169
Ak S., Bilir S., Karaali S., Buser R., Cabrera-Lavers A., 2007b, New Astron., 12, 605
Bensby T., Feltzing S., Lundström I., 2003, A&A, 410, 527
Bensby T., Feltzing S., Lundström I., Ilyin I., 2005, A&A, 433, 185
Bilir S., Karaali S., Ak S., Yaz E., Cabrera-Lavers A., Coşkunoğlu K. B., 2008, MNRAS, 390, 1569
Burnett B. et al., 2011, A&A, 532, 113
Buser R., Rong J., Karaali S., 1999, A&A, 348, 98
Carney B. W., Yong D., Teixera de Almeida M. L., Seitzer P., 2005, AJ, 130, 1111
Chiappini C., Matteucci F., Gratton R., 1997, ApJ, 477, 765
Chiappini C., Matteucci F., Romano D., 2001, ApJ, 554, 1044
Coşkunoğlu B. et al., 2011, MNRAS, 412, 1237
Dehnen W., 1998, AJ, 115, 2384
De Simone R. S., Wu X., Tremaine S., 2004, MNRAS, 350, 627
Dinescu D. I., Girard T. M., van Altena W. F., 1999, AJ, 117, 1792



Downloaded from https://academic.oup.com/mnras/article-abstract/419/4/2844/2908030 by guest on 28 January 2020

Du C., Zhou X., Ma J., Shi J., Chen A. B., Jiang Z., Chen J., 2004, AJ, 128, 2265
ESA, 1997, The *Hipparcos* and *Tycho* Catalogues, ESA SP-1200. ESA, Noordwijk
Famaey B. et al., 2005, A&A, 430, 165
Famaey B., Siebert A., Jorissen A., 2008, A&A, 483, 453
Gilmore G., Wyse R. F. G., 1985, AJ, 90, 2015
Hernquist L., 1990, ApJ, 356, 359
Johnson D. R. H., Soderblom D. R., 1987, AJ, 93, 864
Johnston K. V., Spergel D. N., Hernquist L., 1995, ApJ, 451, 598
Karaali S., Bilir S., Karataş Y., Ak S. G., 2003, PASA, 20, 165
Karataş Y., Klement R. J., 2012, New Astron., 17, 22
Luck R. E., Lambert D. L., 2011, AJ, 142, 136
Luck R. E., Kovtyukh V. V., Andrievsky S. M., 2006, AJ, 132, 902
Luck R. E., Andrievsky S. M., Kovtyukh V. V., Gieren W., Graczyk D., 2011, AJ, 142, 51
Mihalas D., Binney J., 1981, Galactic Astronomy: Structure and Kinematics, 2nd edn. Freeman & Co., San Francisco
Miyamoto M., Nagai R., 1975, PASJ, 27, 533
Munari U., Sordo R., Castelli F., Zwitter T., 2005, A&A, 442, 1127
Nordström B. et al., 2004, A&A, 418, 989
Pauli E. M., 2005, in Gerdjikov V., Tsvetkov M., eds, Prof. G. Manev's Legacy in Contemporary Astronomy, Theoretical and Gravitational Physics. Heron Press Limited, Sofia, Bulgaria, p. 185
Pompéia L. et al., 2011, MNRAS, 415, 1138
Rahimi A., Kawata D., Prieto C. A., Brook C. B., Gibson B. K., Kiessling A., 2011, MNRAS, 415, 1469
Robin A. C., Haywood M., Créze M., Ojha D. K., Bienaymé O., 1996, A&A, 305, 125
Rong J., Buser R., Karaali S., 2001, A&A, 365, 431
Ruchti G. R. et al., 2011, ApJ, 737, 9
Schönrich R., Binney J., 2009, MNRAS, 396, 203
Seabroke G. M. et al., 2008, MNRAS, 384, 11
Shaver P. A., McGee R. X., Newton L. M., Danks A. C., Pottasch S. R., 1983, MNRAS, 204, 53
Siebert A. et al., 2011, AJ, 141, 187
Skuljan J., Hearnshaw J. B., Cottrell P. L., 1999, MNRAS, 308, 731
Soubiran C., Girard P., 2005, A&A, 438, 139
Steinmetz M. et al., 2006, AJ, 132, 1645
Straizys V., Lazauskaite R., 2009, Baltic Astron., 18, 19
Trefzger C. F., Pel J. W., Gabi S., 1995, A&A, 304, 381
Vlajić M., Bland-Hawthorn J., Freeman K. C., 2009, ApJ, 697, 361
Wilson M. L. et al., 2011, MNRAS, 413, 2235
Worthey G., España A., MacArthur L. A., Courteau S., 2005, ApJ, 631, 820
Yaz E., Karaali S., 2010, New Astron., 15, 234
Yong D., Carney B. W., Teixera de Almeida M. L., 2005, AJ, 130, 597
Zwitter T. et al., 2008, AJ, 136, 421

## SUPPORTING INFORMATION

Additional Supporting Information may be found in the online version of this article.

**Table 2.** Stellar atmospheric parameters, astrometric, kinematic and dynamic data for the whole sample.

Please note: Wiley-Blackwell are not responsible for the content or functionality of any supporting materials supplied by the authors. Any queries (other than missing material) should be directed to the corresponding author for the article.

This paper has been typeset from a TEX/LATEX file prepared by the author.

Downloaded from https://academic.oup.com/mnras/article-abstract/419/4/2844/2908030 by guest on 28 January 2020